

# Design, Fabrication, and Characterization of Three-Dimensional Single-Walled Carbon Nanotube Assembly and Applications As Thermal Sensors

S. Selvarasah, *Student Member, IEEE*, A. Busnaina, and M. R. Dokmeci, *Member, IEEE*

**Abstract**—We present the design, fabrication, and characterization of vertical assembly of 3-D single-walled carbon nanotubes (SWNTs) thermal sensors. Carbon nanotubes (CNT) were deposited utilizing dielectrophoretic (DEP) assembly technique with a 98.7% yield. The scanning electron micrograph images revealed that by adjusting the height of the 3-D microelectrodes and the overlap between them allows control over bundle size, number of bundles, and effective length of the sensing elements. The two-terminal resistance of the 3-D devices was reduced by 20% on average from their initial values after the thermal annealing process. The 3-D SWNT thermal sensors were next characterized and a higher temperature coefficient of resistance (TCR) was measured compared to the previously reported DEP aligned CNT-based thermal sensors. The TCR of the single-electrode thermal sensor ranged from  $-0.157\%/^{\circ}\text{C}$  to  $-0.232\%/^{\circ}\text{C}$ , whereas the TCR of the multielectrode sensor varied from  $-0.327\%/^{\circ}\text{C}$  to  $-0.778\%/^{\circ}\text{C}$  measured during the heating cycle. The thermal sensitivities of these 3-D devices were also measured during cooling where the obtained TCR was close to the values obtained during the heating cycle.

**Index Terms**—3-D Assembly, Single-walled carbon nanotubes (SWNTs), thermal sensors.

## I. INTRODUCTION

NANOTECHNOLOGY enables the realization of small, lightweight, inexpensive, and highly sensitive sensors for diverse applications [1]–[3]. Nanoscale materials not only provide greater sensitivity but can also be tailored for specific sensing applications [1]–[4]. Carbon nanotube (CNT), a 1-D nanomaterial, has gained tremendous interest in sensing applications, especially in nanobiotechnology, due to its exceptional physical, mechanical, and chemical properties [4], [5]. CNT, a rolled-up graphene strip, which forms a closed cylinder, is compact,

lightweight and has high aspect ratio. CNTs have high-carrier mobility, large current carrying capability, high mechanical stability, and thermal conductivity. CNTs have been utilized as active sensing elements in different sensing applications, including biosensors [6]–[8], chemical and gas sensors [9], [10], pressure sensors [11], transistors [12], [13], flow sensors [14], and thermal sensors [15], [16]. Single-walled carbon nanotubes (SWNT) with their ultrahigh surface area to volume ratios, striking optical properties, and size-dependent physical properties are more appealing for CNT-based sensors than their multiwalled carbon nanotubes (MWNTs) counterparts [4]. It is worth noting that most efforts up to now utilized planar, 2-D device architectures while realizing nanotube-based sensors and devices.

3-D arrangements of CNTs have been realized and being studied as an attractive alternative to that of 2-D planar techniques since they offer a means for large-scale, higher density realization of novel nanoelectronic devices [17], [18]. Recently, 3-D SWNT structures utilizing porous alumina nanotemplates [19] and field-assisted assembly [20] have been demonstrated. Compared to other assembly methods, the dielectrophoretic (DEP) assembly method provides placement of SWNTs at the desired locations with alignment [21], [22]. Moreover, the DEP assembly process is low-temperature, high yield and is amenable to wafer scale [23], [24] fabrication, and it is shown that it can provide control [25] over the number of assembled nanotubes. Previously, the authors reported a hybrid technique combining both bottom-up DEP assembly and top-down microfabrication techniques to realize room temperature fabrication of 3-D SWNT interconnects [20]. In this paper, we report the characterization of the 3-D vertical assembly of SWNTs and their thermal sensing properties. First, DEP assembly parameters were investigated for a high-yield assembly process, and then the critical dimensions of the microelectrode platform, namely, the overlap and the vertical distance between the electrodes were studied to understand their impact to the number of assembled bundles and the angle of incline of the SWNT sensors. Finally, 3-D thermal sensors were demonstrated using both single and multiple finger electrode structures. Their thermal sensitivity was next characterized during heating and cooling cycles, and it was found that the SWNT sensors displayed higher temperature coefficient of resistance (TCR) compared to previously reported dielectrophoretically aligned CNT-based thermal sensors.

## II. FABRICATION PROCESS

The fabrication process, as illustrated in Fig. 1(a), starts with the deposition and patterning of the first Cr/Au electrode layer

Manuscript received January 8, 2010; accepted December 12, 2010. Date of publication December 23, 2010; date of current version January 26, 2011. This work was supported in part by the Nanoscale Science and Engineering Research Centers Program of the National Science Foundation under Award No. NSF-0425826 and in part by the National Science Foundation under Award No. NER-0608892. The review of this paper was arranged by Associate Editor V. Swaminathan.

S. Selvarasah and M. R. Dokmeci are with the Electrical and Computer Engineering Department, Northeastern University, Boston, MA 02115, USA (e-mail: sselvara@ece.neu.edu; e-mail: mehmetd@ece.neu.edu).

A. Busnaina is with the Mechanical Engineering Department, the National Science Foundation (NSF) Nanoscale Science and Engineering Center for High-Rate Nanomanufacturing, and the NSF Center for Nano and Microcontamination Control, Northeastern University, Boston, MA 02115 USA (e-mail: busnaina@coe.neu.edu).

Color versions of one or more of the figures in this paper are available online at <http://ieeexplore.ieee.org>

Digital Object Identifier 10.1109/TNANO.2010.2101080

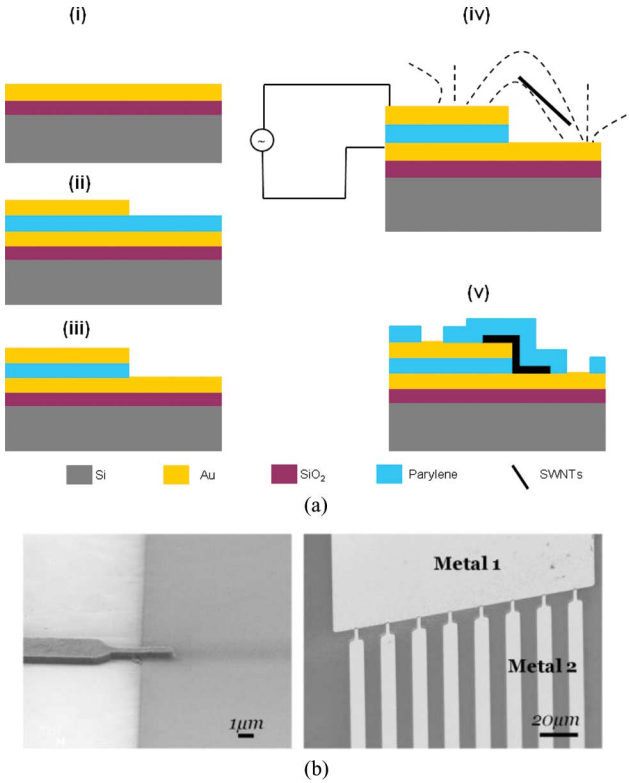


Fig. 1. Microplatforms for 3-D assembly: (a) fabrication process for the micromachined 3-D electrode. (b) SEM micrographs of the fabricated single and multiple (eight) electrode platforms, where these electrodes have a vertical separation of 1  $\mu\text{m}$  and an overlap distance of 3  $\mu\text{m}$ , respectively.

(200 Å/1500 Å) by a liftoff process on an oxidized silicon wafer [see Fig. 1(a-i)]. Then a thin parylene-C dielectric layer was deposited at room temperature. Next, the second metal layer (Cr/Au 200 Å/1500 Å) was deposited and patterned using liftoff technique [see Fig. 1(a-ii)]. These two metal layers form the 3-D electrodes for assembling the SWNTs. Utilizing the second metal layer as a mask, we then etched the parylene-C layer with an inductively coupled plasma (Plasma therm 790) reactor using  $\text{O}_2$  plasma [see Fig. 1(a-iii)]. After fabrication, DEP assembly was utilized to assemble SWNTs between the 3-D electrodes [see Fig. 1(a-iv)]. Finally, a thin layer of parylene-C (1.0  $\mu\text{m}$ ) was deposited as the encapsulation layer and the contacts were opened using the ICP etcher for electrical measurements [see Fig. 1(a-v)]. The scanning electron microscopy images of fabricated single and multiple (eight) finger electrodes are shown in Fig. 1(b), where these electrodes have a vertical separation of 1  $\mu\text{m}$  and an overlap distance of 3  $\mu\text{m}$ , respectively.

In our DEP assembly process, SWNTs in a CMOS grade aqueous solution procured from Nantero, Inc., was utilized. The average diameter and length of these SWNTs were 1.25 nm and 2  $\mu\text{m}$ , respectively. The weight concentration of the SWNT in this aqueous solution was 0.046%, while the pH of the supplied solution was 6.5. The original SWNT solution was first sonicated for 30 min with an ultrasonic cleaner (Branson B-22-4). Subsequently, it was further diluted to the desired CNT concen-

tration with deionized (DI) water and again was sonicated for 2 h prior to the DEP assembly.

### III. EXPERIMENTAL RESULTS AND DISCUSSION

#### A. Dielectrophoretic Assembly of 3D-SWNTs and Two-Terminal Electrical Measurements

In the first set of experiments, the SWNT solution was diluted into 1:1000 with DI water, and assembly experiments were conducted at a frequency of 10 MHz and voltage of 10 Vp-p for 20 s. Devices were inspected under a scanning electron micrograph (SEM) and two-terminal  $I$ - $V$  measurements were performed to verify the electrical continuity between the electrodes. 76 devices were fabricated using these DEP parameters and their assembly yield was next studied. A “good assembly” is defined to be the case where there is an electrical path between the top and the bottom electrodes, which was confirmed by both  $I$ - $V$  measurements and SEM imaging, which revealed that the SWNT bundles formed a bridge between the 3-D microelectrodes, and that there was no damage to the electrodes. Among the 76 devices, 38 devices resulted in good assembly, 5 devices failed ( $I$ - $V$  measurement showed an open connection) and in the other 33 devices, the electrodes were damaged, which resulted in a yield of 50%. SEM images taken from the 33 destroyed devices revealed that the nanotubes clustered together and formed agglomerated structures on the electrodes and/or the top metal electrodes peeled off from the chip. During the assembly of these 33 devices, it was also observed that the initial formation of bubbles on the surface of the 3-D assembly area was followed by the destruction of the electrodes. We believe that the damage to the electrodes was caused by the electrolysis of DI water and also possibly parylene peel off due to joule heating. Electrolysis at the electrode surface occurs at low frequencies and high voltages [26]. Dong *et al.* observed similar bubble formation, which eventually destroyed electrodes at a frequency lower than 50 kHz, and reported that the electrochemical interaction can be avoided at the electrode/solution interface by applying high frequency (1–10 MHz) field [27].

For the next set of assembly experiments, the SWNT solution was diluted to a ratio of 5:1000 with deionized water and assembly was performed with an electric field of 2 Vp-p and a frequency of 10 MHz for 1 min, and 75 devices were made using this recipe. With this new recipe, we have found that our yield went up to 98.7% (74 devices had good assembly whereas one device did not). All 74 devices were inspected under an SEM, and it was observed that none of the electrodes were destroyed. In both assembly processes, 3-D electrodes had a width of 3  $\mu\text{m}$ , an overlap distance of 3  $\mu\text{m}$ , and a vertical separation of 1  $\mu\text{m}$ . The initial 3-D DEP assembly parameters (10 Vp-p, 10 MHz) caused electrolytic dissociation due to the high-electric fields, which formed bubbles on the surface and eventually destroyed the electrode. It was experimentally observed during the second assembly recipe (2 Vp-p and 10 MHz) that the use of an assembly voltage with a smaller amplitude avoided electrolysis and the resulting bubble formation. The use of higher assembly voltages with higher amplitudes resulted in higher electric fields, which induced temperature rise in the fluid due to joule

heating, where the temperature increase ( $\Delta T$ ) is given by

$$\Delta T = \frac{\sigma V^2}{2k} \quad (1)$$

where  $\sigma$  and  $k$  are the electrical and thermal conductivity of the fluid, and  $V$  is the voltage applied between the electrodes [26]. The glass transition ( $T_g$ ) temperature of parylene-C is around  $90^\circ$  [28]. When parylene-C is exposed to a high temperature (above  $T_g$ ), it will experience high stress levels, which is closer to the yield strength of the polymer film (55 MPa). Accordingly, the peeling of the top electrode, which is above the parylene-C dielectric, could also have been caused by the higher temperature generated by the higher electric fields.

The amount of nanotubes assembled across the 3-D electrode can be controlled by scaling the DEP force. The DEP force acting on the CNTs is given by the following equation [31], [32]

$$F_{\text{dep}} = \frac{\pi}{6} r^2 l \varepsilon_m \text{Re} \{K(\omega)\} \nabla E_{\text{rms}}^2 \quad (2)$$

$$K(\omega) = \left( \frac{\varepsilon_p^* - \varepsilon_m^*}{\varepsilon_m^*} \right) \quad (3)$$

where  $l$  and  $r$  are the length and radius of a rod-like particle, respectively,  $\varepsilon_m$  is the real permittivity of the suspending medium,  $E_{\text{rms}}$  is the root mean square (rms) of the electric field, and  $K(\omega)$  is the Clausius–Mosotti factor.

In (2),  $\varepsilon_p^*$  and  $\varepsilon_m^*$  are the complex permittivities of the rod-like particle and the suspending medium, respectively. Here  $\varepsilon^* = \varepsilon - i(\sigma/\omega)$ , where  $i = \sqrt{-1}$ ,  $\varepsilon$  is the real permittivity and  $\sigma$  is the conductivity of the material. In general,  $\varepsilon$  is a material property and can be written as a product of the relative permittivity of the material and permittivity of free space  $\varepsilon_0$ . As shown in (1), the strength of the DEP force is proportional to the size and shape of the nanostructure, electrical properties of the nanomaterial, and suspending medium, as well as the gradient of field squared. In our assembly process, SWNTs are suspended in the aqueous medium (DI water) and the DEP force is proportional to the gradient of field squared. That is, the magnitude of the DEP force scales by the following relationship [29]:

$$|F_{\text{DEP}}| \approx \frac{V^2}{L^3} \quad (4)$$

where  $V$  and  $L$  are the applied voltage and the distance between the electrodes, respectively. Previously, the authors have demonstrated [20] that the density of the assembled nanotubes is proportional to the applied voltage. It was also observed that when a higher voltage was applied between the 3-D electrodes, more nanotubes were assembled around the edges of the tip of the electrode and also formed thicker bundles. We hypothesize that the number of assembled SWNT bundles can be controlled by adjusting the magnitude of the electric field, which can also be done by changing the distance between the electrodes. In the case of 3-D electrodes, the spacing ( $H$ ) and the overlap/separation distance ( $L$ ) between the top and bottom electrodes were varied (see Fig. 2) to understand the interplay between the dimensions of the assembly platform and the number of assembled SWNT bundles.

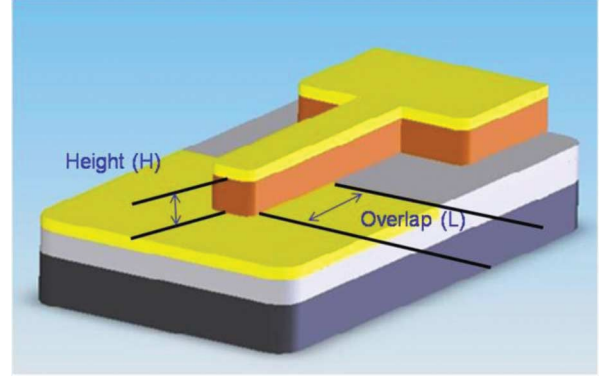


Fig. 2. Schematic drawing of the 3-D assembly electrodes illustrating the height ( $H$ ) and overlap distance ( $L$ ), which can be varied to scale the DEP forces between the top and the bottom electrodes.

Fig. 3 shows a summary of assembly experiments where the vertical distance between electrodes ( $H$ ) was varied from 269, 1052, 2085, and 2828 nm with an overlap distance of about  $3 \mu\text{m}$ . As the distance between the electrodes was reduced, the electric field strength between the top and bottom electrodes increased significantly and caused the formation of thicker SWNT bundles. Moreover, it was also found that as the distance between the top and the bottom electrodes was changed, so did the incline angle and the length of suspended SWNTs bundles. It is evident from Fig. 3(a) that the bundles are more inclined for smaller electrode separation (i.e.,  $H = 269$  nm) than in the case of larger electrode separation (i.e.,  $H = 1052$  nm) as seen in Fig. 3(b). The length of the suspended nanotubes were also longer at  $H = 1052$  nm, whereas a small section of (shorter) tubes formed the bridge for the case where  $H = 269$  nm. During the DEP assembly, the CNTs will align in the direction of electric field lines before assembling in between the electrodes. In other words, the vertical alignment and length of single bundles of SWNTs can be tuned by changing the electric field lines. In the case of a height ( $H$ ) of 269 nm, the shorter separation distance between the top and the bottom electrodes resulted in a stronger electric field, which created a stronger DEP force and allowed the SWNT bundles to move more upright. Utilizing (4), we have calculated the approximate DEP force for each height and the force corresponding to a height ( $H$ ) of 269 nm was about 1162 times higher than the one present for  $H = 2828$  nm (see Table I). Accordingly, shorter bundles were assembled with a steeper angle. In the other case, where the height was 1052 nm, the weaker electric field lines resulted in a less weaker DEP force, and the force experienced by the nanotubes was not strong enough to realize a vertical assembly. SWNTs bundles aligning along the larger electric field lines created less inclined and longer suspended SWNT bundles assembled between the 3-D electrodes. However, when the spacing was above  $1 \mu\text{m}$ , only a small section of bundled nanotubes were suspended near the bottom electrode and the rest followed the sidewall of the parylene-C dielectric, which was caused by the weaker DEP force [see Fig. 3(c), (d)].

The two-terminal  $I$ - $V$  measurements showed an exponential decrease in resistance when the vertical separation (the height

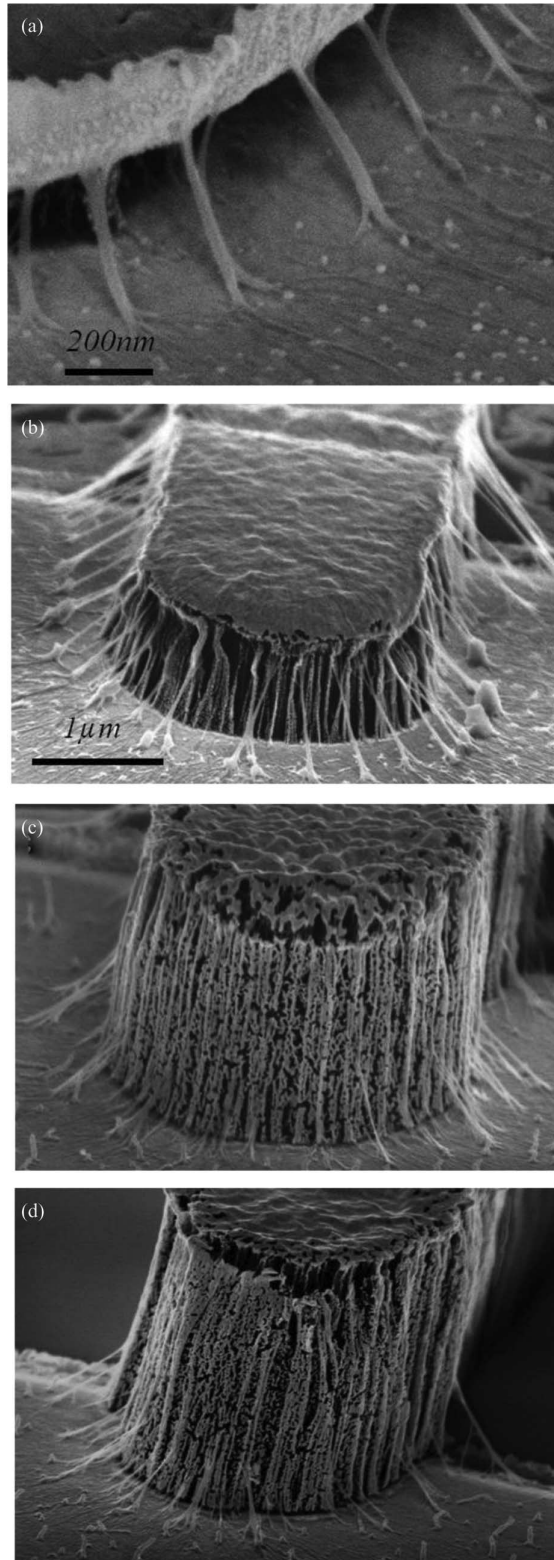


Fig. 3. Adjusting the distance between the top and the bottom electrodes allows control over the magnitude of the electric field. The vertical distance between the 3-D electrodes (thickness of the parylene-C layer) was varied from (a) 269 nm, (b) 1052 nm, (c) 2085 nm, and (d) 2828 nm, where the overlap distance was kept at 3  $\mu\text{m}$ . It is evident from the previously SEM images (a–d) that as the height was reduced the diameter and the angle of incline of the assembled SWNT bundles have increased. Moreover, the length of the suspended 3-D SWNTs decreased when the electrode height was reduced (this was more applicable to  $H \leq 1 \mu\text{m}$ ).

TABLE I  
COMPARISON OF DEP FORCES FOR DIFFERENT MICROELECTRODE GEOMETRIES

Height (nm)	Overlap (nm)	$F_{\text{DEP}}$	$F_{\text{DEP}}^n$
269	3.000	51.4	1162.5
1.052	3.000	0.86	19.45
2.085	3.000	0.11	2.49
2.828	3.000	0.044	1

$F_{\text{DEP}}$  is the calculated DEP force using eqn (2).  $F_{\text{DEP}}^n$  is the normalized DEP force to the smallest value which is obtained at  $H=2,828 \text{ nm}$ .

of the parylene-C thickness) between the electrodes was reduced. Similarly, when the separation (lateral) between the 3-D electrodes was decreased from 2702, 1022, down to 117 nm (electrodes had a vertical separation of 1  $\mu\text{m}$ ), enhanced the DEP force and caused more nanotube bundles to be assembled between the top and the bottom electrodes (see Fig. 4) and also the two-terminal resistance of the 3-D SWNT assemblies decreased exponentially. Furthermore, the top electrode, which was 1022 nm away from the bottom electrode, resulted in seven SWNTs bundles between them [see Fig. 4(a)]. We also found that increasing the overlap distance between the electrodes from 1190 nm [see Fig. 4(c)] to 3290 nm [see Fig. 4(d)] also caused the increase in the number of assembled bundles from 20 to 30. A summary approximate DEP force values calculated using (2) are shown in Table II and confirms our SEM observations.

After a thorough SEM inspection on several 3-D devices with a separation distance of 1  $\mu\text{m}$  or above, it was noticed that (looking from the bottom electrode) the section of the length of the assembled bundles followed the oxide surface and the remaining bent forward on to the top electrode [see Fig. 4(a)]. The 3-D electrode with a separation distance of less than 1  $\mu\text{m}$  always formed bundles inclined where the angle of incline can be adjusted by controlling the height between the electrodes. In addition, the field strength is nearly uniform around the edge of the hemispherical tip at their respective height. When the top electrode begins to overlap with the first electrode, more SWNT bundles assembled around the tip of the electrode as seen in Fig. 4. In summary, by controlling the spacing and the overall/separation distance between the 3-D electrodes allow control in the angle, the bundle thickness, the suspended length, and the number of assembled SWNT bundles around the edges of the tip of the top electrode.

The formation of low contact resistance between CNTs and metal electrodes is essential for their application in nano devices/sensors. Thermal annealing has been demonstrated as one of the simplest methods to improve contact resistance in large scale [30]. After assembly, 3-D devices were annealed at 90  $^{\circ}\text{C}$  for 30 min to improve their contact resistance. The percentage change in two-terminal resistance for seven devices for two different device geometries was studied. The two-terminal resistance decreased between 19%–62% for devices with an overlap distance of 894 nm, whereas an overlap distance of 5484 nm resulted in a reduction of 7%–63%. On the average, a 20% decrease in the two-terminal resistance from its initial value was recorded on most of the devices. After annealing, the devices were encapsulated with a parylene-C layer and contacts were opened for  $I$ – $V$  measurements.

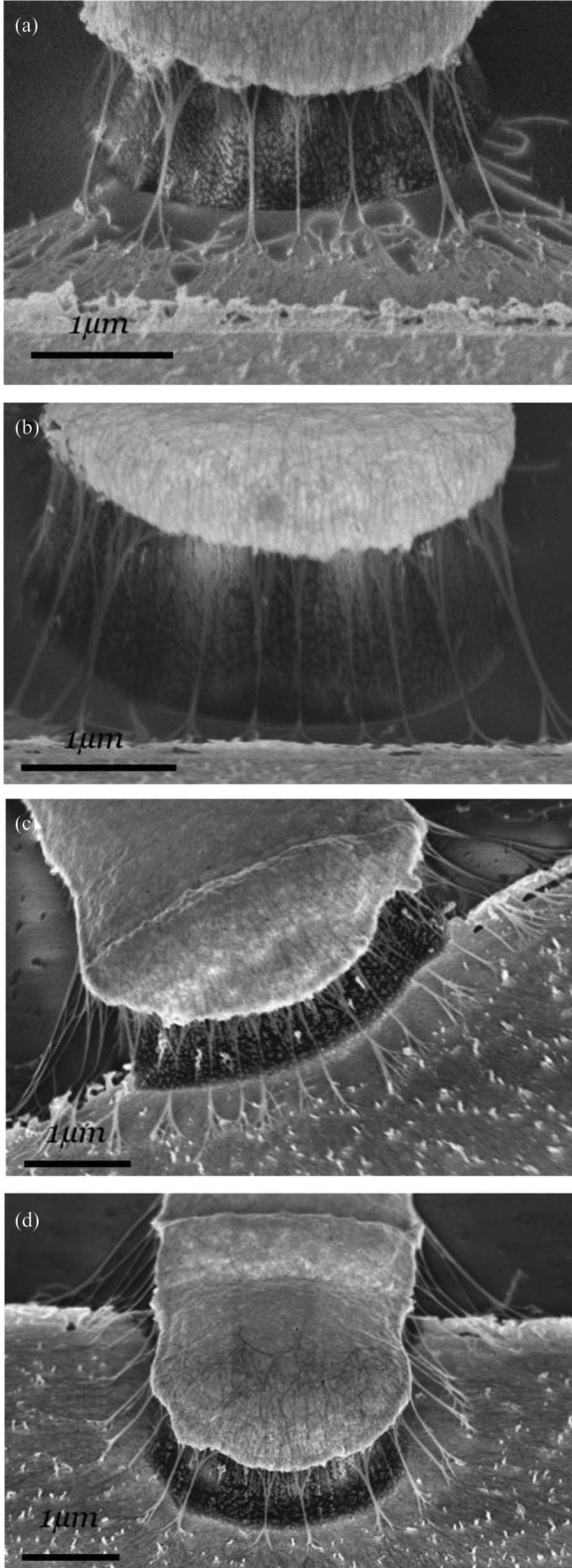


Fig. 4. Overlap distance between the top and bottom electrodes was changed from (a) 1022, (b) 117, (c) 1190 (d) to 3290 nm. As a result, more SWNT bundles assembled around the edges of the hemispherical top electrode as shown in the SEM micrographs through of the 3-D devices (a) to (d), which resulted in 7, 9, 20, and 30 bundles, respectively.

TABLE II  
COMPARISON OF DEP FORCES FOR DIFFERENT MICROELECTRODE GEOMETRIES

Vertical distance (nm)	Overlap (O) Separation (S) (nm)	$F_{DEP}$	$F_{DEP}^n$
1000	2.702 (S)	0.04	1
1000	1.022 (S)	0.34	8.1
1000	117 (S)	0.97	23.2
1000	1.190 (O)	1	23.9
1000	3.290 (O)	1	23.9

$F_{DEP}$  is the calculated DEP force using eqn (2).  $F_{DEP}^n$  is the normalized DEP force to the smallest value which was obtained at Separation=2,702 nm.

### B. Thermal Sensing Properties of 3-D SWNTs

To characterize the 3-D SWNT thermal sensors, we have next placed the devices on an SUSS PM5 analytical probe system with a heatable chuck. First, the temperature of the chuck was ramped up to 65 °C with 10 °C increments every 10 min. Next, it was cooled down to room temperature (25 °C). This thermal annealing cycle was repeated several times in order to stabilize the two terminal  $I$ - $V$  measurements. This process stabilized the resistance readings and was routinely done prior to measurements in CNT-based thermal sensors [15], [16]. During the thermal cycling process it was observed that the two-terminal resistance of the 3-D devices increased, but the measured resistance stabilized after several cyclic measurements. This could potentially be due to the fact that some of the metallic SWNTs may have been burnt during the stabilization process. After the calibration process, the temperature responses of the sensors were investigated. The temperature was varied from 25 °C to 65 °C with 10 °C increments, while the resistance was measured. Fig. 5 displays the measured temperature response from the single and multiple (eight) finger thermal sensors after the stabilization. The two-terminal resistance of single and multiple finger electrodes were 345 Ohms (device1) and 303.7 Ohms (device 2) for single-finger electrode devices, and 45 Ohms (device 1) and 28.3 Ohms (device 2) for multiple finger electrodes devices, respectively. Fig. 6(a), (b) represents the graphs for  $I$ - $V$  measurements of device 2 from the previously mentioned single and multiple electrode devices.

SWNTs are sensitive to temperature and their resistance decreased with increasing temperature. This thermal behavior of the bundled SWNTs are due to the semiconducting nanotubes inside the assembled bundles. Similar temperature behavior of dielectrophoretically assembled nanotubes was previously reported by Chan *et al.* [15] and Chen *et al.* [16]. As the temperature was increased from 25 °C to 65 °C, the resistance decreased by 13.1%–31% on multiple electrode thermal sensor devices, whereas we observed a decrease of 6.3%–9.3% on the single-electrode devices. TCR was calculated based on the following equation [15], [16]:

$$R(T) = R_0(1 + \alpha(T - T_0)) \quad (5)$$

where  $R(T)$  and  $R_0$  are the resistance at temperature  $T$  and at room temperature  $T_0$  and  $\alpha$  is the TCR.

This temperature response study was conducted with both single and multiple electrode 3-D sensors, and the respective TCR values were calculated during the heating cycle. The TCR value of the single-electrode devices varied from  $-0.157\%/^{\circ}\text{C}$  to  $-0.232\%/^{\circ}\text{C}$ , whereas the TCR of the multiple electrode sensors

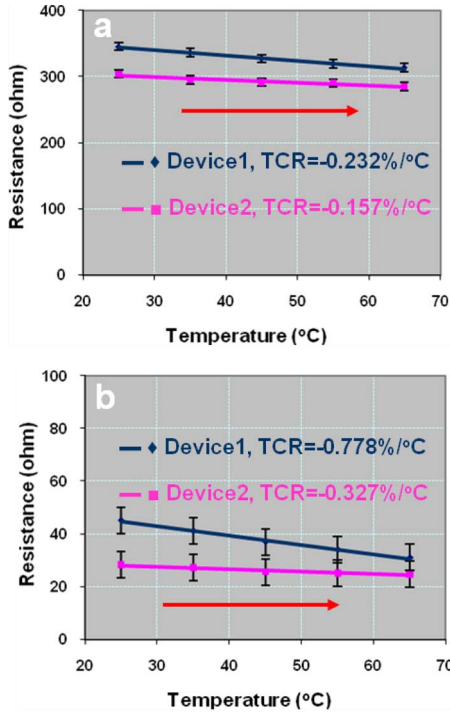


Fig. 5. Measured resistance versus temperature plots from a single-electrode and a multiple electrode 3-D thermal sensors during the heating cycle. The temperature was varied from 25 °C to 65 °C with 10 °C increments and the two terminal resistance of the devices was continuously recorded. (a) TCR ranged from  $-0.157\%/^{\circ}\text{C}$  to  $-0.232\%/^{\circ}\text{C}$  for a single-electrode 3-D thermal sensor, whereas (b) the multi electrode devices displayed a TCR of  $-0.327\%/^{\circ}\text{C}$  to  $-0.778\%/^{\circ}\text{C}$ .

varied from  $-0.327\%/^{\circ}\text{C}$  to  $-0.778\%/^{\circ}\text{C}$ . Comparing our data with the previously reported DEP assembled 2D MWNT [15] and SWNT [16] based thermal sensors, we were able to achieve higher sensitivity. Single-finger 3-D thermal sensor displayed more than twice the sensitivity of that from Chen *et al.*'s single-gap SWNT thermal sensor (the dimension of their single gap: gap = 800 nm, height = 150 nm, and length = 4.5  $\mu\text{m}$ ). The multiple electrode thermal sensor device exhibited more than three times the sensitivity compared to their multigap (five) 2-D sensor [16]. Next, we remeasured the thermal behavior of our 3-D sensor while reducing the temperature from 65 °C to 25 °C with 10 °C decrements. During this cooling cycle, thermal sensitivity was measured for device1 and is shown in Fig. 7 for both single and multiple electrode sensors. The TCR value of the single-electrode thermal sensor was  $-0.213\%/^{\circ}\text{C}$  [see Fig. 7(a)], whereas the TCR of the multielectrode sensor  $-0.795\%/^{\circ}\text{C}$  [see Fig. 7(b)]. Even though their resistance has slightly increased, their TCR values closely matched with that of the TCR values, as seen in Fig. 5, obtained during the heating cycle. This electrical hysteresis during heating and cooling process can be attributed to purification of SWNTs and/or destruction of metallic SWNTs during the multiple heating processes [33]. It is likely that during the heating cycles, the defects initially present in the assembled SWNT bundles were removed. Furthermore, dielectrophoretically deposited SWNTs consist of both metallic and semiconducting SWNTs, and these metallic nanotubes reduced the temperature dependence of the sensor and caused the

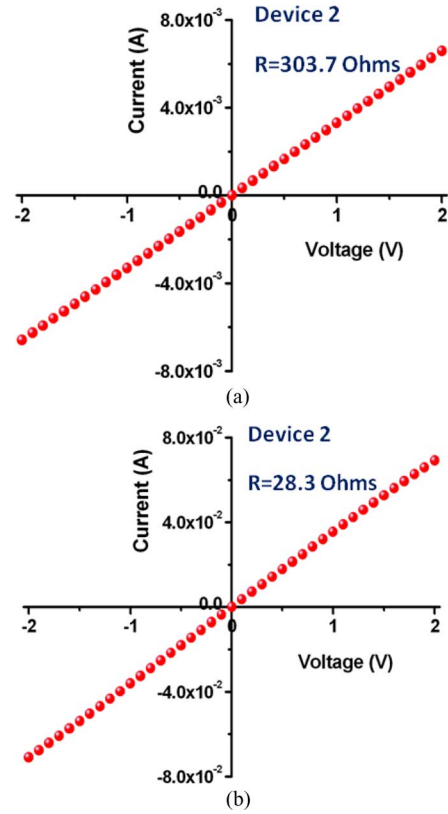


Fig. 6.  $I$ - $V$  measurement of device 2. Two-terminal resistances measured from (a) single and (b) multiple electrode 3-D devices are 303.7 and 28.3 Ohms, respectively.

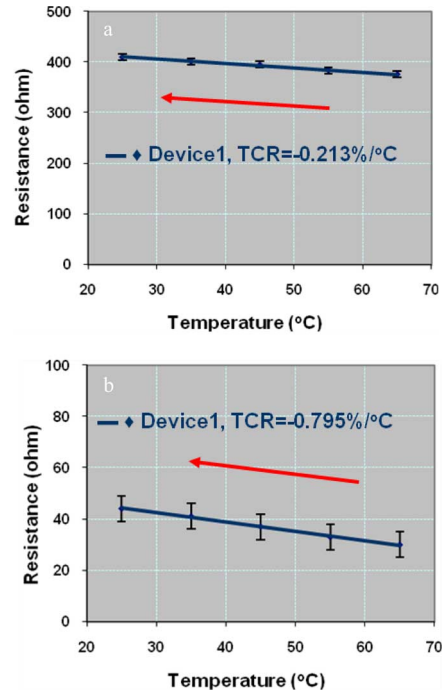


Fig. 7. Temperature versus resistance relationship (for device 1 in Fig. 5) was studied during the cooling cycle, where the temperature was varied from 65 °C to 25 °C with 10 °C decrements. The TCR of the single-electrode (a) and multiple electrode (b) thermal sensors ranged from  $-0.213\%/^{\circ}\text{C}$  and  $-0.795\%/^{\circ}\text{C}$ , respectively.

sensitivity to vary during the measurements [34]. A reliable and highly sensitive 3-D thermal sensor can be achieved by exclusive use of semiconducting SWNTs.

The performance of an ideal sensor is determined by key factors, such as high sensitivity and reliability, low power consumption, lightweight, low cost, and high volume manufacturing (batch fabrication). CNTs with their attractive properties are promising candidates for the realization of next generation of sensors. Using CNTs as a thermal sensing element, we have demonstrated a highly sensitive 3-D miniaturized thermal sensor, which would find vast applications in the sensing industry. This 3-D sensor can be utilized in biomedical industry as an implantable sensor to monitor temperature, automobile, and aviation industry to acquire (vehicle) temperature. It can also be used inside aqueous environments as a temperature measurement tool and integrated thermal sensor for other nanomechanical systems, microelectromechanical systems, bio and nanodevices. This 3-D SWNTs-based thermal sensor is an attractive alternative to existing temperature sensing materials, such as vanadium oxide, polysilicon, etc.

#### IV. CONCLUSION

In this paper, we presented the 3-D assembly of SWNTs and a 3-D SWNT-based thermal sensor. DEP assembly parameters were optimized for a high yield (98.7%) process, and scaling the geometry of 3-D microelectrode platform enabled the control over number of assembled bundles, angle of incline, and the length of suspended SWNT bundles. 3-D devices were annealed at 90 °C for 30 min to improve their contact resistance. An average of at least 20% decrease in their two-terminal resistance was observed after the thermal annealing process. Finally, the thermal sensitivity of both single and multiple 3-D electrode sensors was measured, and the TCR value of the single-electrode thermal sensor had a range from  $-0.079\%/^{\circ}\text{C}$  to  $-0.232\%/^{\circ}\text{C}$ , whereas the TCR of the multiple electrode sensor varied from  $-0.526\%/^{\circ}\text{C}$  to  $-0.778\%/^{\circ}\text{C}$ .

#### ACKNOWLEDGMENT

The authors would like to thank Nantero, Inc., and Brewer Science, Inc., for supplying with CMOS grade single-walled carbon nanotubes solution. This research was conducted at the George J. Kostas Nanoscale Technology and Manufacturing Research Center at Northeastern University.

#### REFERENCES

- [1] G. M. Whitesides, "The 'right' size in nanobiotechnology," *Nat. Biotechnol.*, vol. 21, pp. 1161–1165, 2003.
- [2] L. Wang, W. Zhao, and W. Tan, "Bioconjugated silica nanoparticles: Development and applications," *Nano Res.*, vol. 1, pp. 99–115, 2008.
- [3] C. R. Lowe, "Nanobiotechnology: The fabrication and applications of chemical and biological nanostructures," *Curr. Opin. Chem. Biol.*, vol. 10, pp. 428–434, 2000.
- [4] Z. Liu, S. Tabakman, K. Welsher, and H. Dai, "Carbon nanotubes in biology and medicine: In vitro and in vivo detection, imaging and drug delivery," *Nano Res.*, vol. 2, pp. 85–120, 2009.
- [5] P. Avouris, Z. Chen, and V. Perebeinos, "Carbon-based electronics," *Nature Nanotechnol.*, vol. 2, pp. 605–615, 2007.
- [6] J. C. Claussen, A. D. Franklin, A. U. Haque, D. M. Porterfield, and T. S. Fisher, "Electrochemical biosensor of nanocube-augmented carbon nanotube networks," *ACS Nano*, vol. 3, pp. 37–44, 2009.
- [7] R. J. Chen, H. C. Choi, S. Bangsaruntip, E. Yenilmez, X. Tang, Q. Wang, Y.-L. Chang, and H. Dai, "An investigation of the mechanisms of electronic sensing of protein adsorption on carbon nanotube devices," *J. Amer. Chem. Soc.*, vol. 126, pp. 1563–1568, 2004.
- [8] A. Star, J.-C. P. Gabriel, K. Bradley, and G. Gruner, "Electronic detection of specific protein binding using nanotube FET devices," *Nano Lett.*, vol. 3, pp. 459–463, 2003.
- [9] J. Kong, N. R. Franklin, C. Zhou, M. G. Chapline, S. Peng, K. Cho, and H. Dai, "Nanotube molecular wires as chemical sensors," *Science*, vol. 287, pp. 287–292, 2000.
- [10] J. Li, Y. Lu, Q. Ye, M. Cinke, J. Han, and M. Meyyappan, "Carbon nanotube sensors for gas and organic vapor detection," *Nano Lett.*, vol. 3, pp. 929–933, 2003.
- [11] C. Stampfer, T. Helbling, D. Oberfell, B. Schoiberle, M. K. Tripp, A. Jungen, S. Roth, V. M. Bright, and C. Hierold, "Fabrication of single-walled carbon-nanotube-based pressure sensors," *Nano Lett.*, vol. 6, pp. 233–237, 2006.
- [12] S. J. Tans, A. R. M. Verschueren, and C. Dekker, "Room-temperature transistor based on a single carbon nanotube," *Nature*, vol. 393, pp. 49–52, 1998.
- [13] R. Martel, T. Schmidt, H. R. Shea, T. Hertel, and P. Avouris, "Single- and multi-wall carbon nanotube field-effect transistors," *Appl. Phys. Lett.*, vol. 73, p. 2447, 1998.
- [14] S. Ghosh, A. K. Sood, and N. Kumar, "Carbon nanotube flow sensors," *Science*, vol. 299, pp. 1042–1044, 2003.
- [15] R. H. M. Chan, C. K. M. Fung, and W. J. Li, "Rapid assembly of carbon nanotubes for nanosensing by dielectrophoretic force," *Nanotechnology*, vol. 15, pp. S672–S677, 2004.
- [16] Z. Chen, Z. Wu, L. Tong, H. Pan, and Z. Liu, "Simultaneous dielectrophoretic separation and assembly of single-walled carbon nanotubes on multigap nanoelectrodes and their thermal sensing properties," *Anal. Chem.*, vol. 78, pp. 8069–8075, 2006.
- [17] G. S. Duesberg, A. P. Graham, M. Liebau, R. Seidel, E. Unger, F. Kreupl, and W. Hoenlein, "Growth of isolated carbon nanotubes with lithographically defined diameter and location," *Nano Lett.*, vol. 3, no. 2, pp. 257–259, 2003.
- [18] W. B. Choi, J. U. Chu, K. S. Jeong, E. J. Bae, J.-W. Lee, J.-J. Kim, and J.-O. Lee, "Ultrahigh-density nanotransistors by using selectively grown vertical carbon nanotubes," *Appl. Phys. Lett.*, vol. 79, no. 22, pp. 3696–3698, 2001.
- [19] E. Gultepe, D. Nagesha, B. D. Frederic Casse, S. Selvarasah, A. Busnaina, and S. Sridhar, "Large scale 3D vertical assembly of single-wall carbon nanotubes at ambient temperatures," *Nanotechnology*, vol. 19, p. 455309, 2008.
- [20] P. Makaram, S. Selvarasah, X. Xiong, C.-L. Chen, A. Busnaina, N. Khan-duja, and M. R. Dokmeci, "Three-dimensional assembly of single-walled carbon nanotube interconnects using dielectrophoresis," *Nanotechnology*, vol. 18, p. 395204, 2007.
- [21] R. Krupke, F. Hennrich, H. B. Weber, M. M. Kappes, and H. V. Lohneysen, "Simultaneous deposition of metallic bundles of single-walled carbon nanotubes using ac-dielectrophoresis," *Nano Lett.*, vol. 3, pp. 1019–1023, 2003.
- [22] S. Banerjee, B. E. White, L. Huang, B. J. Rego, S. O'Brien, and I. P. Herman, "Precise positioning of single-walled carbon nanotubes by AC dielectrophoresis," *J. Vac. Sci. Technol. B*, vol. 24, pp. 3173–3178, 2006.
- [23] A. Vijayaraghavan, S. Blatt, D. Weissenberger, M. Oron-Carl, F. Hennrich, D. Gerthsen, H. Hahn, and R. Krupke, "Ultra-large-scale directed assembly of single-walled carbon nanotube devices," *Nano Lett.*, vol. 7, pp. 1556–1560, 2007.
- [24] A. H. Monica, S. J. Papadakis, R. Osianer, and M. Paranjape, "Wafer-level assembly of carbon nanotube networks using dielectrophoresis," *Nanotechnology*, vol. 19, p. 085303, 2008.
- [25] L. An and C. R. Friedrich, "Real-time gap impedance monitoring of dielectrophoretic assembly of multiwalled carbon nanotubes," *Appl. Phys. Lett.*, vol. 92, p. 173103, 2008.
- [26] A. Castellanos, A. Ramos, A. González, N. G. Green, and H. Morgan, "Electrohydrodynamics and dielectrophoresis in microsystems: Scaling laws," *J. Phys. D: Appl. Phys.*, vol. 36, pp. 2584–2597, 2003.
- [27] L. Dong, V. Chirayos, J. Bush, J. Jiao, V. M. Dubin, R. V. Chebani, Y. Ono, J. F. Conley, Jr., and B. D. Ulrich, "Floating-potential dielectrophoresis-controlled fabrication of single-carbon-nanotube transistors and their electrical properties," *J. Phys. Chem. B*, vol. 109, pp. 13148–13153, 2005.

- [28] T. Goda, T. Konno, M. Takai, and K. Ishihara, "Photoinduced phospholipid polymer grafting on parylene film: advanced lubrication and antibiofouling properties," *Colloids Surf. B.*, vol. 54, no. 1, pp. 67–73, 2007.
- [29] T. B. Jones, *Electromechanics of Particles*. New York: Cambridge University Press, 1995.
- [30] J.-O. Lee, C. Park, J.-J. Kim, J. Kim, J. W. Park, and K.-H. Yoo, "Formation of low-resistance ohmic contacts between carbon nanotube and metal electrodes by a rapid thermal annealing method," *J. Phys. D: Appl. Phys.*, vol. 33, pp. 1953–1956, 2000.
- [31] M. Dimaki and P. Boggild, "Dielectrophoresis of carbon nanotubes using microelectrodes: A numerical study," *Nanotechnology*, vol. 15, pp. 1905–2102, 2004.
- [32] L. X. Benedict, S. G. Louie, and M. L. Cohen, "Static polarizabilities of single-wall carbon nanotubes," *Phys. Rev. B*, vol. 52, pp. 8541–8549, 1995.
- [33] L. Valentini, L. Lozzi, C. Cantalini, I. Armentano, J. M. Kenny, L. Ottaviano, and S. Santucci, "Effects of oxygen annealing on gas sensing properties of carbon nanotube thin films," *Thin Solid Films*, vol. 436, pp. 95–100, 2003.
- [34] M. E. Itkis, F. Borondics, A. Yu, and R. C. Haddon, "Bolometric infrared photoresponse of suspended single-walled carbon nanotube films," *Science*, vol. 312, pp. 413–416, 2006.



**Selvapraha Selvarasah** (S'08) received the B.Sc. degree in computer engineering from McMaster University, Hamilton, ON, Canada, in 2002, and the M.S. degree in electrical engineering from Northeastern University, Boston, MA, in 2008, where he is currently working toward the Ph.D. degree at the Electrical and Computer Engineering Department.

In his five years of graduate study at Northeastern University, he has authored and/or coauthored 17 peer-reviewed technical journal articles and 40 conference publications. He has presented his research

work nationally and internationally, and has one patent application. His research articles were highlighted in the journal cover of *Nanotechnology* 2007 and NSTI Nanotechnology program guide 2008. His contribution to research is recently highlighted by Northeastern graduate studies Web site. His H-index is six. His current research interests include micronano fabrication, nanomaterials and electronic devices, flexible electronics, nanoscale integration, organic field effect transistors, and BioMEMS.

Mr. Selvarasah is a Student Member of Eta Kappa Nu and Materials Research Society (MRS). He has received several awards including the MRS Best Poster Award in 2007, and the winner of the outstanding graduate student award from Northeastern University in 2009.



**Ahmed Busnaina** received the Ph.D. degree from Oklahoma State University.

He is currently the William Lincoln Smith Chair Professor and the Director of the National Science Foundation (NSF) Nanoscale Science and Engineering Center for High-Rate Nanomanufacturing and the NSF Center for Nano and Microcontamination Control at Northeastern University, Boston, MA. He is internationally recognized for his work on nano- and microscale defects mitigation and removal in semiconductor fabrication. He also involved in the fabrication

of nanoscale wires, structures, and interconnects. He specializes in directed assembly of nanoelements (such as nanotubes and nanoparticles) and in the fabrication of micro- and nanoscale structures. Research support exceeded 25

million dollars. He served as a consultant on microcontamination and particle adhesion issues to the semiconductor industry. He is the author or coauthor of more than 300 papers in journals, proceedings, and conferences. He organized more than 80 conferences, workshops, symposia, and programs for many professional societies, chaired and organized more than 90 sessions and panels.

Prof. Busnaina is a Fellow of the American Society of Mechanical Engineers and the Adhesion Society, a Fulbright Senior Scholar and listed in Who's Who in the World, in America, in science and engineering, etc. He also serves on many advisory boards including Samsung Electronics; Chemical Industry Nanomaterials Roadmap, International Technology Roadmap for Semiconductors, the *Journal of Particulate Science and Technology*, the *Journal of Environmental Sciences*, the *Semiconductor International*, the *Journal of Advanced Applications in Contamination Control*. He was the recipient of the 2006 Nanotech Briefs National Nano 50 Award, Innovator category, the 2006 Outstanding Faculty, Søren Buus Outstanding Research Award, Northeastern University 2006, and the 2005 Aspiration Award, Northeastern University.



**Mehmet R. Dokmeci** (M'00) received the B.S. (with distinction) and M.S. degrees from the University of Minnesota, Minneapolis, and the Ph.D. degree from the University of Michigan, Ann Arbor, all in electrical engineering.

His dissertation was on hermetic encapsulation of implantable microsystems for chronic use in living systems. Since Fall 2004, he has been with the Electrical and Computer Engineering Department, Northeastern University, Boston, MA, as an Assistant Professor. He was an Assistant Research Scientist in the

Electrical Engineering and Computer Science Department, University of Michigan, Ann Arbor, where he developed a Pb-Sn solder-based wafer-level vacuum packaging technology. He has three and half years of industrial experience at Corning-Intellisense Corporation, Wilmington, MA, developing microelectromechanical systems -based products for the telecommunications and life sciences industries. He is the author or coauthor of 31 journal articles, 77 conference publications, and 2 book chapters. He holds two patents. His current research interests include concentrated in all areas of micro and nanomachining and its applications to biomedical and optical devices, nanoscale integration, flexible electronics, and implantable biosensors.

Dr. Dokmeci is a member of the American Association for the Advancement of Science, the Materials Research Society (MRS), and the American Chemical Society. He and his students received numerous awards for their research including the Best Poster Award at the 8th IEEE International Conference on Nanotechnology in 2008, the Best Poster Award at the MRS Fall Meeting in 2007, and the Best Poster Award at the Annual Northeastern University Tech Expo in 2008, 2009. His research was also featured on the cover of *Nanotechnology* during 2007 and 2009.